

THE INFLUENCE OF AN INITIAL TWISTING ON TAPERED BEAMS UNDERGOING LARGE DISPLACEMENTS

G. Migliaccio¹ and G. Ruta²

¹ Civil and Industrial Engineering, University of Pisa;
National Group for Mathematical Physics, Pisa
Largo Lucio Lazzarino 2, 56122, Pisa, Italy
e-mail: giovanni.migliaccio.it@gmail.com

² Structural and Geotechnical Engineering, University “La Sapienza”;
National Group for Mathematical Physics, Roma
Via Eudossiana 18, I-00184, Roma, Italy
e-mail: giuseppe.ruta@uniroma1.it

Abstract. *The behaviour of pre-twisted and tapered beams (such as turbine or helicopter blades) is characterized by stress distributions that may be quite different from those of the usual beam theory, yielding couplings among bending, twisting and traction. We propose a physical-mathematical model for tapered beams that accounts for the effects of the pre-twist of the cross-sections along the centre-line. The beam centre-line may undergo large displacements, while its cross-sections see small warping both in- and out of their plane. Supposing infinitesimal strain, a variational approach provides the field equations, which are perturbed in terms of a small geometric ratio and shall be solved numerically in general. However, analytical closed-form solutions exist in some cases, such as for isotropic beams with pre-twisted, bi-tapered elliptic cross-sections; they are presented and compared with the results of nonlinear 3D-FEM simulations.*

Keywords: pre-twist, tapered beams, variational approach, small-parameter perturbation.

1 INTRODUCTION

Non-prismatic beams, e.g., blades of propellers, helicopters and wind turbines, components of civil buildings and bridges, require continuous efforts to improve their description and enhance their performance and cost effectiveness. This is because their cross-sections have non-uniform geometry (taper) and may be initially twisted, making the usual beam theory inadequate. The geometric pre-twist, for example, introduces couplings in their structural response, making bending always three-dimensional, and traction not independent from torsion [1-6]. A review on this topic is that by Rosen [7], while Kunz [8] presents a survey on beam theories

for rotor blades, comparing models for rotating beams and discussing how engineering theories for rotor blades evolved over the years. The taper also contributes to the couplings among flexure, traction, and torsion. Wind blades are a noteworthy example in which such couplings emerge, as they may be pre-twisted, tapered, and even curved in their unstressed state, and may undergo large displacements [9-12]. Thus, their modelling is very challenging and does not generally provide analytical closed-form formulas for design purposes. On the other hand, the formulas of the usual beam theory, based on Saint-Venant's solutions, usually provide incorrect results for non-prismatic cases, as the authors also found in a recent work [12].

A rational model for beams is due to Love [13]; recent studies are: [14-16], where geometrically exact models are introduced, derived from three-dimensional continua, with a view towards numerical implementation; [17], where a discussion on the elastic energy stored in a deformed beam is provided; [18], investigating how the cross-section stress and strain are approached by a variational method; [19], where non-infinitesimal strains are considered; [20], where non-linear elastic coupling between inner actions is considered; [21], investigating tapered elements; [22], discussing various kinematic representations for beams modelling; [23-24], highlighting the inadequacies of usual design formulas for tapered beams; and a paper by the authors [25], introducing a beam model derived from three-dimensional continua and suitable for the above quoted engineering applications; reviews are in [7-8,26-27].

General non-prismatic beams still require investigations to obtain stress and strain by a rigorous, yet application-oriented, model; indeed, the cross-section pre-twist and taper and the centre-line curvature should be explicitly considered; in addition, one should not limit to small displacements, even though usual formulas should be recovered in the trivial cases.

This paper extends previous works by the authors [11,12,25] in that it considers the effects of the geometric pre-twist on the behaviour of bi-tapered beams undergoing large displacements of the axis, in- and out-of-plane cross-sectional warping and small strains. The main objective is the evaluation of the effects of the pre-twist superposed to those of the taper on the stress and strain fields in such structural elements. The model for the aforementioned beams is introduced in Section 2. Analytical results for beams with pre-twisted, bi-tapered cross-sections are presented in Section 3. Numerical examples, comparisons with nonlinear 3D-FEM simulations, and thorough comments are reported in Section 4.

2 MECHANICAL MODEL

We sketch the model presented in [12], where further details are available. We then investigate the influence of the cross-sections' pre-twist on the fields equations, discuss how these equations may be solved, and search cases where it is possible to find analytical closed-form results for non-prismatic beams with pre-twisted, bi-tapered cross-sections.

2.1 Geometry and strain measures

Our beam is a collection of plane figures (the transverse cross-sections) attached at a 3D curve (the centre-line or axis) through one of their points (in the following sections, when specified, such point is considered to be the cross-section centroid). The cross-sections are fully deformable, i.e. they may undergo in- and out-of-plane distortions (referred to generally as warping); then, the displacement of each material point from the reference to the current state consists of a rigid part (analogously to usual theories of beams with rigid cross-sections) onto which warping is superimposed. Thus, it is possible to consider the axis motion to be finite regardless of the amplitude of the warping and strain fields, which are considered infinitesimal (as is specified in the following). Henceforth, Greek (Latin) indices range from 2 to 3 (from 1 to 3); repeated indices imply summation over their range.

Fig. 1 shows a sketch of the beam reference (left) and current (right) shapes. Two local triads of orthogonal unit vectors are introduced: the first, b_i , is in the reference state, with b_1 tangent to the reference axis (i.e. the cross-section is orthogonal to the centre-line in the reference state), and depends on the reference arc-length s , i.e. $b_i=b_i(s)$. The second triad, a_i , is an image of b_i in the current state and depends on s and the evolution parameter t , i.e. $a_i=a_i(s,t)$. A third triad c_i pertains to a fixed Cartesian reference frame with origin at will.

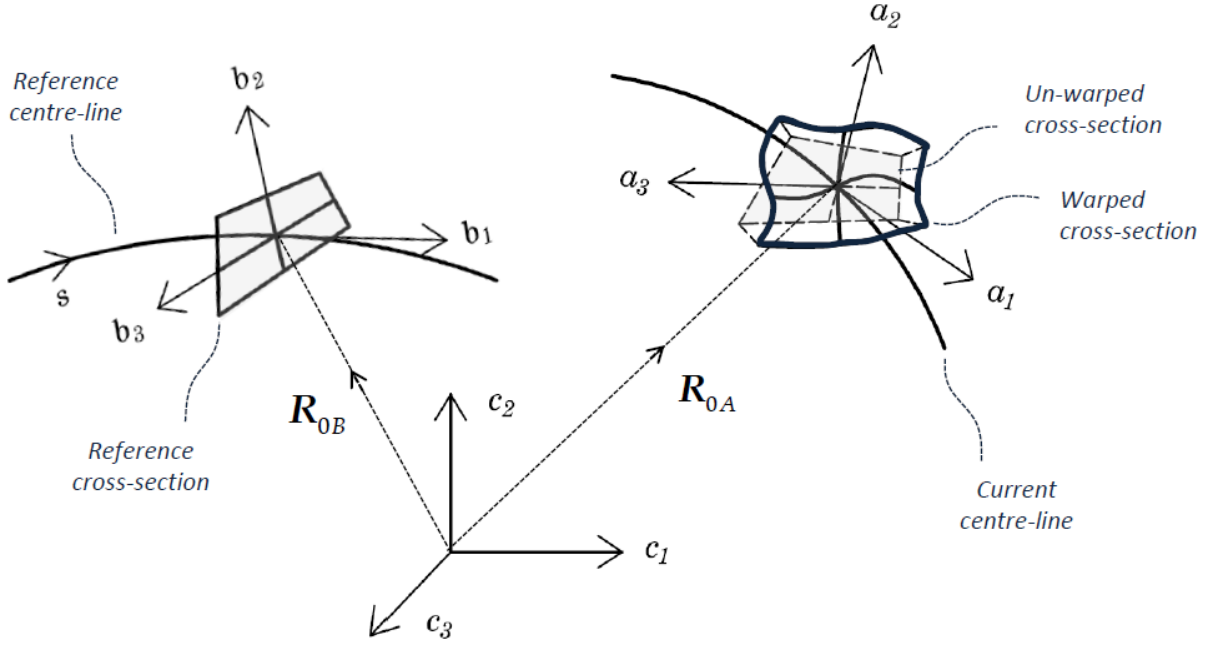


Figure 1: Sketch of reference and current states: axes, cross-sections, local and global bases.

The mapping functions R_A and R_B identify the position of the beam material points in the current and reference states, respectively. The reference mapping function is

$$R_B(z_i) = R_{0B}(z_1) + x_\alpha(z_i)b_\alpha(z_1) \quad (1)$$

where R_{0B} denotes the position of the reference axis relative to the triad c_i , x_α identify the position of the points in the cross-section relative to axis, and z_i are three variables independent of time, with $z_1=s$ and z_α belonging to a bi-dimensional domain mapping the prototype of the cross-section. The spanwise variation of the cross-sections reference shape is given by

$$x_i = \Lambda_{ij}z_j \quad (2)$$

where the Λ_{ij} depend on z_1 ; we consider beams with bi-tapered cross-sections for which it is $\Lambda_{11}=1$, $\Lambda_{22}=\Lambda_2(z_1)$, $\Lambda_{33}=\Lambda_3(z_1)$, while the remaining Λ_{ij} vanish identically.

The current mapping function is, analogously to Eq. (1),

$$R_A(z_i, t) = R_{0A}(z_1, t) + x_\alpha(z_i)a_\alpha(z_1, t) + w_k(z_i, t)a_k(z_1, t) \quad (3)$$

where R_{0A} denotes the position of the current axis relative to the triad c_i , while the w_k are the components of the warping vector, w , relative to triad a_k . In this way, we are separating the in- and out-of-plane motion of the cross-sections (described by w) from the displacement of the beam's axis (associated to the difference between R_{0A} and R_{0B}). The former can thus be small (as specified in the following) regardless of the latter (which may be large).

Since the local triads are of unit vectors, a measure of the local curvatures of the reference and actual axes are the vector fields k_B, k_A given by $b'_i = k_B \wedge b_i$ and $a'_i = k_A \wedge a_i$, where the apex prime denotes the derivative with respect to s and \wedge is the usual cross-product.

The vector field k , describing the curvature variation between the current and reference states, is then given by

$$k = T^T k_A - k_B \quad (4)$$

where the proper orthogonal tensor field $T = a_i \otimes b_i$, with \otimes the usual tensor (dyadic) product, defines the relative orientation between the triads a_i and b_i ; k_B, k_A, k depend on s .

The vector field γ describes the difference between the tangent vectors to the current and reference axes and is defined as

$$\gamma = T^T R'_{0A} - R'_{0B} \quad (5)$$

It can be shown that γ and k vanish for rigid motions and are invariant under superposed rigid motion [15,20] (i.e., they are objective). We refer to them as 1D strain measures, while the Green-Lagrange tensor E is referred to as 3D strain measure. The latter is written, as in [12], in a form based on the assumption of small strain and warping. In fact, we assume that: the characteristic dimension h of the cross-sections is much smaller than the reference length L of the centre line (i.e., the beam is slender); the axial curvatures are much smaller than $1/h$ (this conforms to standard assumptions on the axial radius of curvature which is considered sufficiently large compared to the cross-sectional diameter [28]); the warping components w_k are small in the sense that they are of the order of $h\varepsilon$, $\varepsilon \ll 1$ being a non-dimensional parameter, and their derivative with respect to z_l has magnitude proportional to $\varepsilon h/L$, thus much smaller than ε . In general, all 1D and 3D strain measures are supposed to have order of magnitude at most ε . The strain tensor E is then expressed, as in [12], in the form

$$E \simeq \frac{T^T H + H^T T}{2} - I \quad (6)$$

where H is the gradient of the transformation between the reference and actual shapes

$$H = \frac{\partial R_A}{\partial R_B} \quad (7)$$

2.2 Stress measures and balance equations

The stress fields in the beam can be determined supposing it to be elastic; for small strain, the second (symmetric) Piola-Kirchhoff stress tensor S is expressed in terms of E as

$$S = 2\mu E + \lambda \text{tr} E I \quad (8)$$

where μ and λ are two known parameters for a given isotropic material [29] and I is the identity tensor. For small strain and warping, it is $P=TS$ and $C=TS T^T$, where P and C are the first Piola-Kirchhoff and the Cauchy stress tensor, respectively.

The stress resultants on transverse cross-sections are a force F and a moment M , both vector fields depending on s ; they are defined by means of P

$$\begin{aligned} F &= \int_{\Sigma} P_{i1} a_i \\ M &= \int_{\Sigma} x_{\alpha} P_{i1} a_{\alpha} \wedge a_i \end{aligned} \quad (9)$$

where Σ is the domain of a transverse cross-section and the components $P_{ij} = P \cdot a_i \otimes b_j$. Here, and in the following, the area of integration is implicit in the integral, that is, the integration is performed over the domain reported in the integral's subscript. The same short-hand notation is used for the volume integrals as well.

We use the principle of expended power to get the balance equations for the considered body, which we think three-dimensional and hyper-elastic [30]. We admit that its interactions with the environment are quantifiable, for each velocity field attainable by the body, by a linear functional of the velocity in the volume V of the reference shape, called external power Π_e

$$\Pi_e = \int_V b \cdot v + \int_{\partial V} p \cdot v \quad (10)$$

In Eq. (10) b is the body force per unit reference volume, p is the contact force per unit area of the reference boundary and v is the referential description of the time rate of the current positions of the body material points, given by

$$v = v_0 + \omega \wedge x_{\alpha} b_{\alpha} + w' \quad (11)$$

In Eq. (11) w' is the time rate of warping, v_0 is the time rate of the position R_{A0} , and ω is related to the time rate of the orientation of the current local triad a_i by $a_i' = \omega \wedge a_i$.

The interactions among parts of the body are quantified by the internal power Π_i

$$\Pi_i = \frac{d}{dt} \int_V \Phi \quad (12)$$

where $\Phi=(S \cdot E)/2$ is the energy density of the body, depending on 1D strains and 3D warping.

According to the principle of expended power, for any velocity field attainable by the body, its interactions with the external environment and among its different parts are such that at any value of the evolution parameter t the total power vanishes or, equivalently, $\Pi_e=\Pi_i$.

The exploitation of such principle is a usual technique in continuum mechanics to obtain balance equations in terms of the unknowns of the problem [20,28-30]; in our case we get

$$\begin{aligned} F' + F_s &= 0 \\ M' + R'_{0A} \wedge F + M_s &= 0 \end{aligned} \quad (13)$$

where F_s and M_s are the resultants per unit length of the beam axis of the external body and contact actions in the current state.

The principle of expended power makes it also possible to reduce the determination of the warping fields to those that verify the following variational statement (as in [12])

$$\delta \int_V \Phi = 0 \quad (14)$$

where the symbol δ denotes the variation operator with respect to the warping fields, related to the time rate in Eq. (12). The warping fields satisfying Eq. (14) can be obtained by solving the corresponding Euler-Lagrange equations [31] by numerical methods (in general) or by analytical approaches yielding closed-form results (in particular cases). Thus, the resolution of the original 3D problem is reduced to that of two problems: the first is defined over the reference cross-section domain and is solved (numerically or, in particular cases, analytically) once and for all for a given cross-section shape; the second is defined over the beam centre-line (i.e., it is expressed by non-linear ordinary differential equations) and must be solved for each single assigned external load. This procedure of course reduces the computational effort and promises to be effective with an aim towards design, as discussed in [12].

In the following we show analytical results indicating the effect of pre-twist on bi-tapered beams (Sect. 3), along with examples that are compared with 3D-FEM results (Sect. 4).

3 ANALYTICAL RESULTS

We find expressions for the stress, strain and warping fields by exploiting condition (14). Indeed, we choose, for easier calculations, that the unit vector a_l is tangent to the current centre-line. The transformation of the cross-section from its reference setting is thus described only

by the functions w_k ; that is, shear strains are accounted for by the warping functions. Warping functions satisfying (14) are determined by solving the corresponding Euler-Lagrange equations up to terms of order $\varepsilon h/L$, similarly to [12]. From a procedural standpoint, in order to write such equations we have to express the energy function Φ in terms of the warping fields and their partial derivatives. To this end, we just have to combine Eq. (1)-(7), which provide the Green-Lagrange strains as functions of the warping fields and their partial derivatives, with Eq. (8), which provides the stress tensor S in terms of the strain tensor E ; further details can be found in [12]. That done, writing the aforementioned equations is just a matter of calculations and is performed by exploiting standard mathematical techniques of calculus of variation (see [31], for instance). The final result of this procedure is reported hereafter and is a system of partial differential equations (PDEs) with Neumann-type boundary conditions, the solution of which provides the components of tensor E .

Note that in this section we focus only on the effects of pre-twist in tapered beams, while other geometric effects (e.g. those of the beam's curvature) are not considered. Proceeding in this way, we obtain the following expressions for the components E_{11}, E_{21}, E_{31} of E , describing the out-of-plane deformations of the transverse cross-sections,

$$\begin{aligned} E_{11} &= k_2 x_3 - k_3 x_2 + \gamma_1 + u_{1,1} + k_{B1} (x_3 u_{1,2} - x_2 u_{1,3}) \\ 2E_{21} &= u_{1,2} - k_1 x_3 + 2(1+\nu)(k_2 x_3 - k_3 x_2 + \gamma_1)(\Lambda_2^{-1} \Lambda_2' x_2 - k_{B1} x_3) + e_2 \\ 2E_{31} &= u_{1,3} + k_1 x_2 + 2(1+\nu)(k_2 x_3 - k_3 x_2 + \gamma_1)(\Lambda_3^{-1} \Lambda_3' x_3 + k_{B1} x_2) + e_3 \end{aligned} \quad (15)$$

where $E_{ij} = E \cdot b_i \otimes b_j$ and ν is Poisson's ratio. In Eq. (15), the comma indicates the derivative with respect to x_i , while the scalar fields e_1, e_2, e_3 are solutions of the Neumann problems

$$\begin{aligned} e_{1,22} + e_{1,33} &= 0 \quad \text{in } \Sigma \\ (e_{1,2} - k_1 x_3)n_2 + (e_{1,3} + k_1 x_2)n_3 &= 0 \quad \text{on } \partial\Sigma \end{aligned} \quad (16)$$

$$\begin{aligned} e_{2,2} + e_{3,3} &= f_2 x_2 + f_3 x_3 \quad \text{in } \Sigma \\ e_{3,2} - e_{2,3} &= g_2 x_2 + g_3 x_3 + g_1 \quad \text{in } \Sigma \\ e_2 n_2 + e_3 n_3 &= 0 \quad \text{on } \partial\Sigma \end{aligned} \quad (17)$$

The fields e_1, e_2, e_3 are a combination of the fields w_k and their partial derivatives with known functions, and make it possible to arrange the consequences of Eq. (14) in the compact form expressed by Eq. (16)-(17), which resemble those for torsion and flexure in a Saint-Venant's cylinder [32]. In such equations, Σ and $\partial\Sigma$ are the cross-section and its boundary; n_α are the

components of the outward unit normal to $\partial\Sigma$; f_α , g_k are linear functions of the strain measures k_α and their s -derivative, and depend on the taper coefficients A_2 , A_3 and pre-twist k_{B1} ,

$$\begin{aligned}
 f_2 &= +2(1+\nu)k'_3 + 2(1+\nu)\left(\Lambda_3^{-1}\Lambda'_3 + 2\Lambda_2^{-1}\Lambda'_2\right)k_3 \\
 f_3 &= -2(1+\nu)k'_2 - 2(1+\nu)\left(\Lambda_2^{-1}\Lambda'_2 + 2\Lambda_3^{-1}\Lambda'_3\right)k_2 \\
 g_1 &= 2k_{B1}(2+2\nu)\gamma_1 \\
 g_2 &= -2\nu k'_2 - 2(1+\nu)\Lambda_2^{-1}\Lambda'_2 k_2 - 2k_{B1}(3+2\nu)k_3 \\
 g_3 &= -2\nu k'_3 - 2(1+\nu)\Lambda_3^{-1}\Lambda'_3 k_3 + 2k_{B1}(3+2\nu)k_2
 \end{aligned} \tag{18}$$

We also get the expressions for the components E_{22} , E_{33} , E_{23} of E , describing the in-plane cross-sections distortion, plus the relevant PDE problem. Hereafter we do not provide details on this but focus on the effects of pre-twist on tapered beams, included in e_1 , e_2 , e_3 .

Given the strain fields (15), we determine the corresponding stress fields by the constitutive Eq. (8) and, subsequently, the stress resultants by eq. (9). We note that the components F_1 , M_2 , M_3 of the stress resultants require the expressions for the strain components E_{11} , E_{12} , E_{13} and the additional term $E_{SV}=E_{22}+E_{33}+2\nu E_{11}$, related to the cross-section in-plane deformation. However, E_{SV} is of higher order with respect to other terms in the expressions of the stress resultants [11], and vanishes in prismatic beams [13, 32-33]. Hereafter, we neglect it in calculating F_1 , M_2 , M_3 ; the components F_i , M_i of the resultant force and moment with respect to the current local triad a_i are then found to be

$$\begin{aligned}
 F_1 &= YA\gamma_1 + YZ_1k_1 + YX_1k'_1 \\
 F_2 &= -YJ_3k'_3 + YJ_{23}k'_2 - YI_3k_3 + YI_{23}k_2 \\
 F_3 &= YJ_2k'_2 - YJ_{23}k'_3 + YI_2k_2 - YI_{32}k_3 \\
 M_1 &= GJ_1k_1 + YV_1\gamma_1 + YV_2k_2 - YV_3k_3 + YH_2k'_2 - YH_3k'_3 \\
 M_2 &= YJ_2k_2 - YJ_{23}k_3 + YZ_2k_1 + YX_2k'_1 \\
 M_3 &= YJ_3k_3 - YJ_{23}k_2 - YZ_3k_1 - YX_3k'_1
 \end{aligned} \tag{19}$$

where Y and G are Young and shear moduli, and the coefficients multiplying 1D strains and their s -derivatives depend on the beam reference shape and Poisson's ratio; their expressions are obtained by combining Eq. (8)-(9), relating the stress resultants and the strain fields (15), with Eq. (15)-(18), providing the strain fields (see appendix). Remark that shearing forces depend on the variation in curvature, which, on their turn, directly affect the problems (16)-(18) that determine the warping functions and hence the local shearing (see appendix).

We now present solutions of the problems (16)-(18) generalizing the results shown in [12].

3.1 The effect of pre-twist on bi-tapered beam with elliptic cross-sections

For generic cross-sections, the problems (16)-(18) require a numerical resolution, as expected, since only few analytical formulas are available even in the linear theory of prismatic beams [13]. For pre-twisted beams with bi-tapered elliptic cross-sections, however, we obtain the following analytical closed-form solutions

$$\begin{aligned}
 e_1 &= m_1 x_2 x_3 \\
 e_2 &= + \frac{m_\alpha x_\alpha x_3}{d_3^2 \Lambda_3^2} + \frac{m_3 + f_2 d_2^2 \Lambda_2^2}{2} \left(\frac{x_2^2}{d_2^2 \Lambda_2^2} + \frac{x_3^2}{d_3^2 \Lambda_3^2} - 1 \right) + \frac{g_1 d_2^2 x_3}{\rho^2 d_3^2 + d_2^2} \\
 e_3 &= - \frac{m_\alpha x_\alpha x_2}{d_2^2 \Lambda_2^2} - \frac{m_2 - f_3 d_3^2 \Lambda_3^2}{2} \left(\frac{x_2^2}{d_2^2 \Lambda_2^2} + \frac{x_3^2}{d_3^2 \Lambda_3^2} - 1 \right) - \frac{g_1 d_3^2 x_2}{d_3^2 + \rho^{-2} d_2^2}
 \end{aligned} \tag{20}$$

where d_2, d_3 are the major semi-axes of a given ellipsis (e.g., the initial cross-section), $\rho = A_3/A_2$ is a known function of s , and the coefficients m_i are given by

$$\begin{aligned}
 m_1 &= \frac{d_3^2 - \rho^{-2} d_2^2}{d_3^2 + \rho^{-2} d_2^2} k_1 \\
 m_2 &= \frac{g_2 + \rho^2 f_3}{1 + 3\rho^2} \Lambda_3^2 d_3^2 \\
 m_3 &= \frac{g_3 - \rho^{-2} f_2}{1 + 3\rho^{-2}} \Lambda_2^2 d_2^2
 \end{aligned} \tag{21}$$

Replacing Eq. (20), (21) into Eq. (15) yields the strain components, then the corresponding stress fields by Eq. (8). It turns out that the 3D strain and stress fields explicitly depend on geometry by the taper functions A_2, A_3 and the pre-twist k_{B1} . The relevant terms can be fundamental to accurately predict the stress and strain fields in non-prismatic beams. Eventually, the force and moment stress resultants in terms of 1D strain measures are given by Eq. (19)

$$\begin{aligned}
 F_1 &= YA\gamma_1 + Y(J_0 - J_1)k_{B1}k_1 \\
 F_2 &= -YJ_3k_3' - YJ_3'k_3 - YJ_2k_{B1}k_2 \\
 F_3 &= YJ_2k_2' + YJ_2'k_2 - YJ_3k_{B1}k_3 \\
 M_1 &= GJ_1k_1 + Y(J_0 - J_1)k_{B1}\gamma_1 \\
 M_2 &= YJ_2k_2 \\
 M_3 &= YJ_3k_3
 \end{aligned} \tag{22}$$

where A, J_0, J_1 , and J_α are, respectively, the cross-section area, polar moment of inertia, Saint-Venant's torsion inertia, and central principal moments of inertia (see appendix).

Eq. (22) are a particular case of Eq. (19) and show, among the rest, the expected coupling of extension and torsion due to the pre-twist. This important effect, studied by many researchers, is confirmed by experimental investigations [1-6]; yet, remark that this result holds for pre-twisted, bi-tapered beams without the need to enforce *ad-hoc* kinematic assumptions on displacements, which are very common in other works (e.g. [6]).

It is important to remark that the effect of the pre-twist is present also in the dependence of the shearing forces on the bending curvatures, absent in usual beams; for the same forces the effect of taper emerges in the derivatives of the moments of inertia along the axis. Remark that the hypothesis of slender beam naturally implies that the shearing force has a constitutive dependence on the bending curvatures, like the one derived in the one-dimensional theory of purely flexible beams and in Saint-Venant's solutions for a straight cylinder. Finally, the analytical results presented here generalize those of the linear theory of prismatic beams (see, e.g., [32-33]) and reduce to the latter for prismatic beams with small centre-line deflection.

As expected by a look at the problems (16)-(18), analytical results such as (20) are found for very few cross-section shapes, but numerical methods for all other cases might be used.

4 NUMERICAL EXAMPLES

The accuracy of the proposed approach is discussed here by means of numerical examples, where we also provide comparisons with the results from nonlinear 3D-FEM simulations.

In order to determine the current state of the considered beams we need to determine the cross-sections warping and the displacements of their axes. The latter are obtained by solving a non-linear set of ordinary differential equations governed by the kinematic, constitutive and balance equations introduced in Sect. 2, which can be numerically integrated with respect to the arc-length s ; further details are in [12].

Hereafter we show the results of the present model for the axis displacement, 1D and 3D strain measures, and 3D stress fields, implemented in a numerical code in MATLAB, here referred to as 3D-BLM. These are compared with those from 3D-FEM simulations performed with ANSYS by a fine mesh of solid tetrahedral elements with 10 nodes and quadratic displacement behaviour [34], to show the effectiveness of the proposed approach.

4.1 Test cases

The tests address a pre-twisted, bi-tapered beam with elliptic cross-sections (Fig. 2), fixed at one end (the root) and loaded at the other (the tip) by a transverse force of increasing magni-

tude. In this case we can use the analytical solution in Sect. 3, included in the numerical model. The length of the axis is 100m, that of the major semi-axes at the root is $d_2=2m$ (edgewise) and $d_3=2m$ (flapwise). The other cross-sections change according to the taper coefficients in Fig. 2 and are pre-twisted linearly from 0deg at the root section to 20deg at the tip section. The material properties are Young's modulus, 70GPa, and Poisson's ratio, 0.25; the load at the tip is a flapwise force F ranging from 100kN to 1500kN, as shown in Fig. 3.

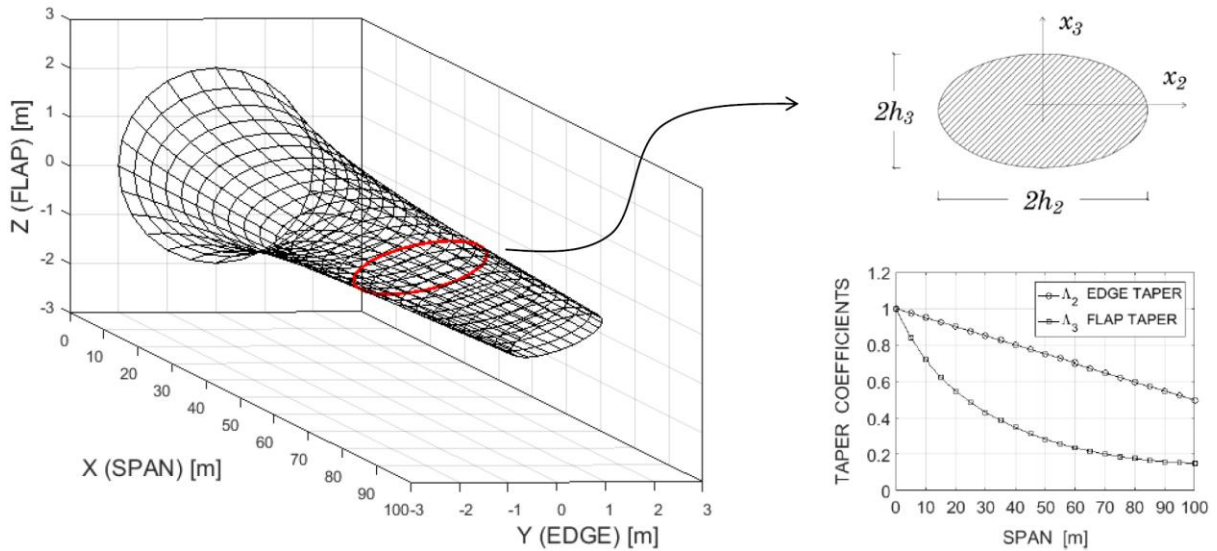


Figure 2: Pre-twisted, bi-tapered beam (left), intermediate section (semi-axes h_2-h_3) and taper coefficients (right).

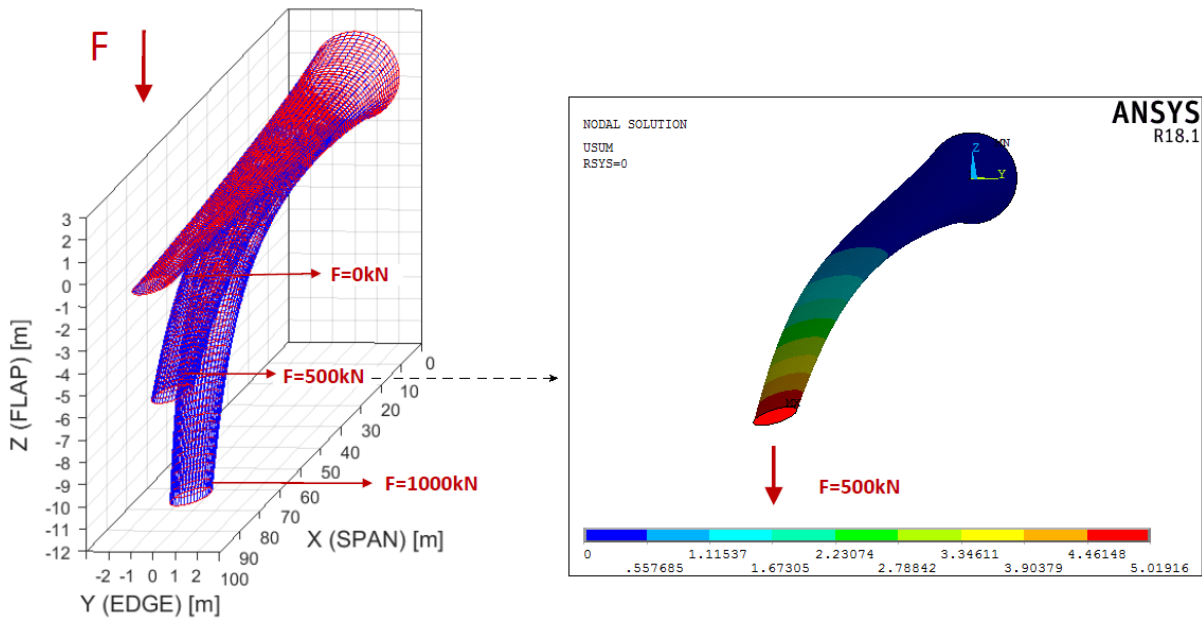


Figure 3: Deflected shapes using 3D-BLM for increasing F (left) and 3D-FEM for $F=500kN$ (right).

The results obtained from 3D-BLM are summarized in Fig. 3 (left), showing an overview of the un-deformed state ($F=0$) and the deformed states for $F=500\text{kN}$ and $F=1000\text{kN}$. Fig. 3 (right), on the other hand, shows the deformed state for $F=500\text{kN}$ given by 3D-FEM.

In general, 3D-BLM provides several information on the response of the beam: axis displacement, change in curvatures, 3D stress and strain fields, stress resultants. Fig. 4 to Fig. 14 provide comparisons between 3D-BLM and 3D-FEM in terms of displacement, strain and stress fields, confirming the computational efficiency and accuracy of 3D-BLM compared to 3D-FEM results. This was already highlighted in previous investigation of the authors, among which [12], where, however, only taper was accounted for.

Specifically, Fig. 4 (left) shows the axis displacement as the tip-force F grows from 100kN to 1500kN . Comparisons with 3D-FEM simulations were done; Fig. 4 (right) reports those for $F=1000\text{kN}$ and $F=1500\text{kN}$. It is worth noting that the tip-displacement is not along the applied tip-force, as expected due to pre-twist: one component is along y (that is, orthogonal to F) and vanishes if the pre-twist is zero, as in the un-twisted cases investigated in [12].

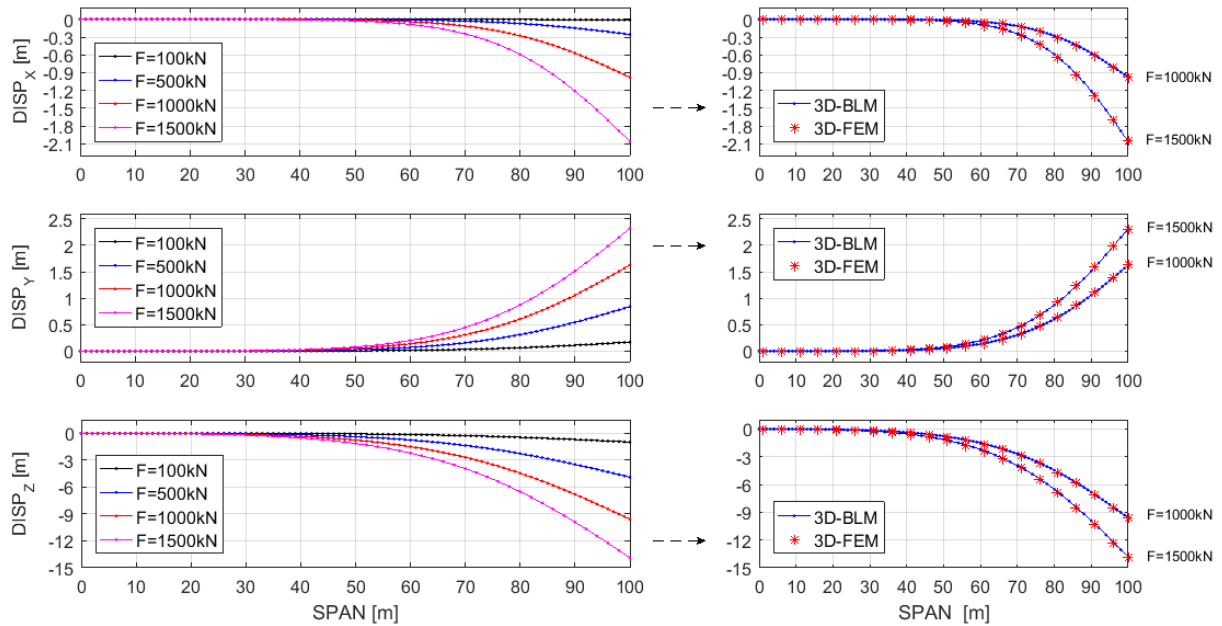


Figure 4: Centre-line displacement by: 3D-BLM for increasing F (left); 3D-FEM for $F=1000\text{-}1500\text{kN}$ (right).

In addition, pre-twist affects the stress and strain fields, hence the stress resultants, by the additional terms proportional the pre-twist k_{BI} in Eq. (16)-(18), (20). An idea of the effect of such additional terms is in Fig. 5 and 6, showing the Cauchy stress C_{YX} at three cross-sections (30%, 50%, 70% span) along one major axis, for $F=100\text{kN}$ and $F=500\text{kN}$, respectively. Blue

lines plot the results of 3D-BLM, including the effects of pre-twist. Black lines plot the results of the same model, neglecting pre-twist, whence the label 3D-BLM-NTW. Red marks denote the results of 3D-FEM simulations. Comparisons between 3D-BLM and 3D-FEM confirm the importance of the terms related to the pre-twist coefficient k_{BI} in Eq. (16)-(18) and (20) for accurate predictions of the stress and strain fields in pre-twisted, bi-tapered beams.

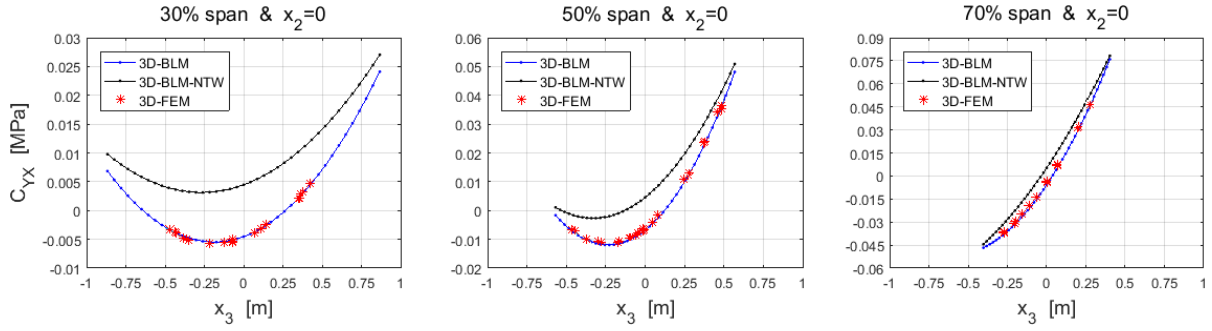


Figure 5: Pre-twist effects on C_{YX} in the cross-sections at 30%, 50%, 70% span for $F=100\text{kN}$.

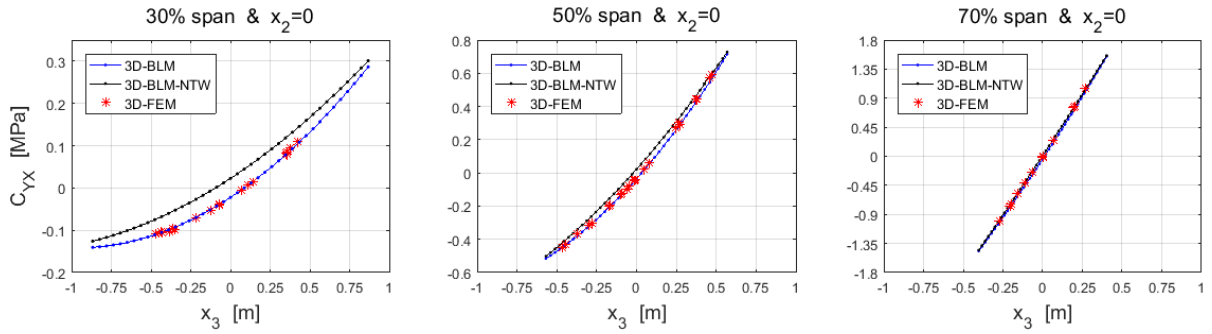


Figure 6: Pre-twist effects on C_{YX} in the cross-sections at 30%, 50%, 70% span for $F=500\text{kN}$

The effects of pre-twist are superimposed to those of taper, i.e.: *i*) a spanwise variation in the cross-section rigidities, affecting the axis deflection and, in turn, stress and strain. This is accounted for through the taper functions A_2, A_3 , acting as scaling factors for the rigidities, and we name it here as taper scaling effect; *ii*) a spanwise variation in the taper coefficients, accounted for through the s -derivative of the taper functions, directly affecting strain and stress, see Eq. (17)-(18). This effect is referred to here as taper derivative effect.

An idea of the output of these effects is in Fig. 7 and 8, showing the Cauchy stress C_{ZX} for the same cross-sections and loads as in Fig. 5, 6. The results of 3D-BLM (blue lines) include both scaling and derivative effects; the latter is neglected in black line plots, whence the label 3D-BLM-NTD. Comparisons of 3D-BLM and 3D-FEM (red marks) confirm the importance of the derivative effects, unpredictable by the theory of prismatic beams.

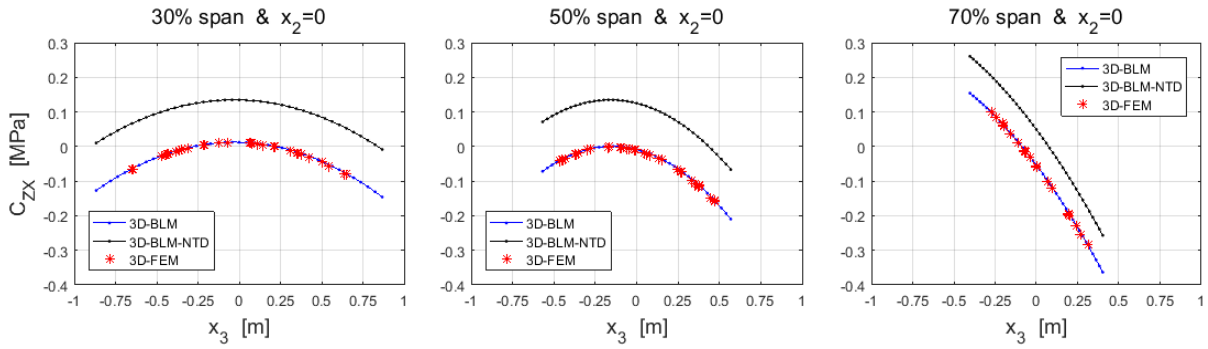


Figure 7: Taper effects on C_{ZX} in the cross-sections at 30%, 50%, 70% span for $F=100\text{kN}$

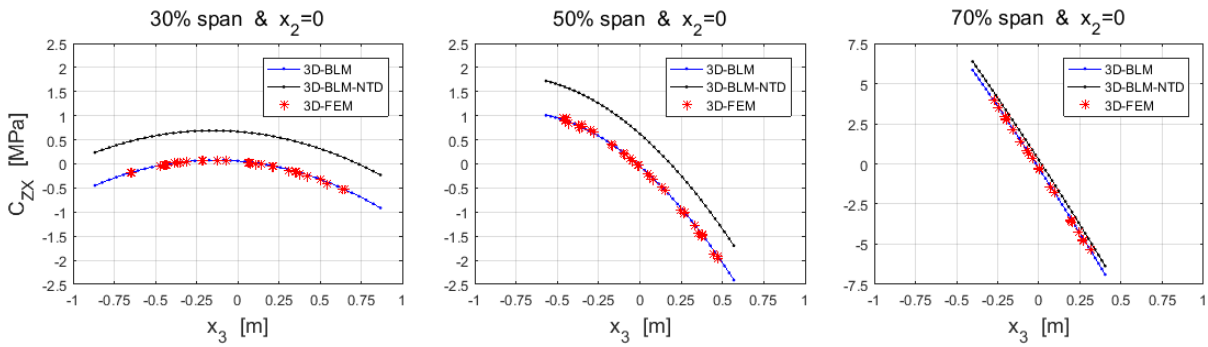


Figure 8: Taper effects on C_{ZX} in the cross-sections at 30%, 50%, 70% span for $F=500\text{kN}$

Further comparisons between 3D-BLM and 3D-FEM are in terms of the Cauchy stresses C_{XX} , C_{YX} , C_{ZX} . In particular, Fig. 9, 10, 11 report the longitudinal stress C_{XX} and the transverse shear stresses C_{YX} , C_{ZX} , respectively, at the same reference cross-sections for $F=500\text{kN}$. It is remarkable to see that the proposed model almost exactly matches the 3D-FEM results obtained by a commercial code, yet requiring less computational time also when pre-twist is included: indeed, the computation is up to a hundred times faster than that of 3D-FEM, just like in [12] for the case of just tapered beams.

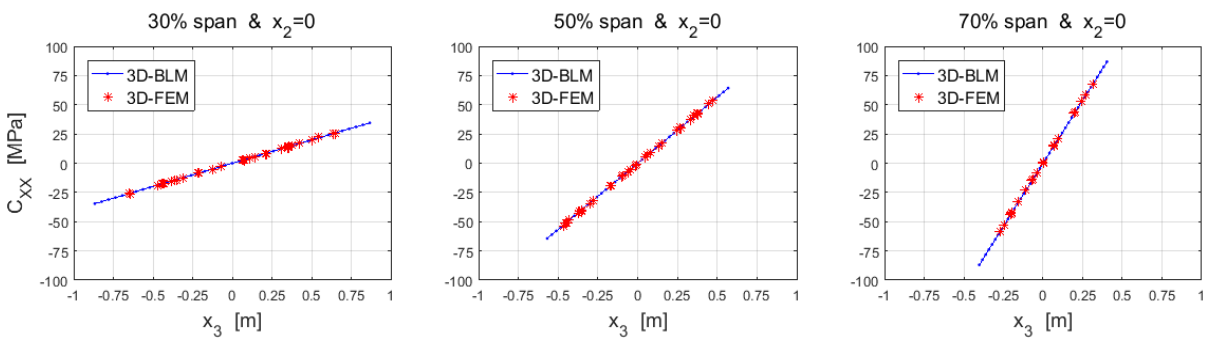


Figure 9: Longitudinal stress C_{XX} in the cross-sections at 30%, 50%, 70% span for $F=500\text{kN}$.

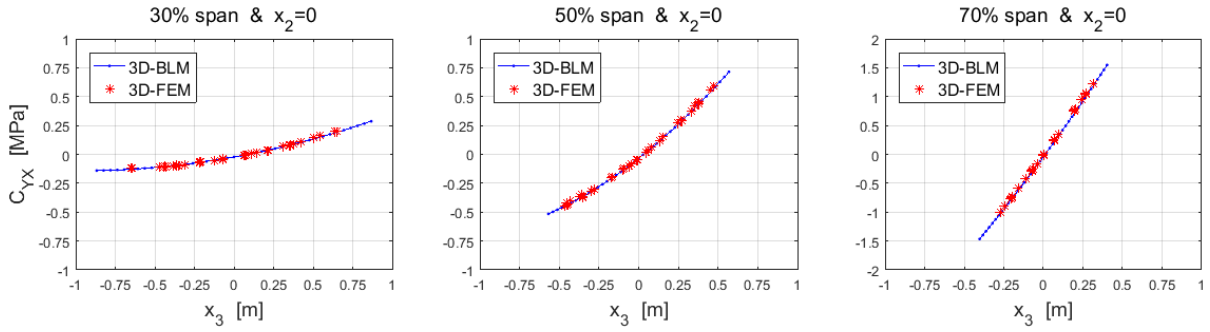


Figure 10: Transverse shear stress C_{YX} in the cross-sections at 30%, 50%, 70% span for $F=500\text{kN}$.

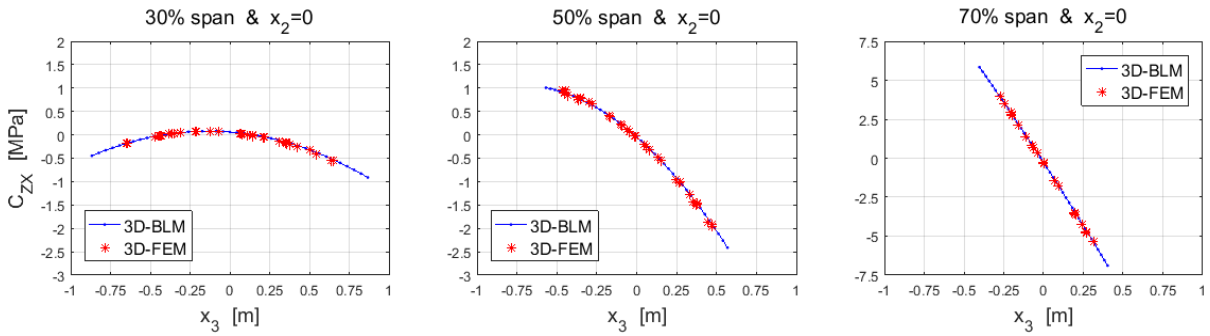


Figure 11: Transverse shear stress C_{ZX} in the cross-sections at 30%, 50%, 70% span for $F=500\text{kN}$.

Similar results are provided for $F=1000\text{kN}$ and are shown in Fig. 12, 13, 14 respectively for C_{XX} , C_{YX} , C_{ZX} . It is apparent how the results match almost exactly those of non-linear 3D-FEM, corroborating the reliability of the proposed model.

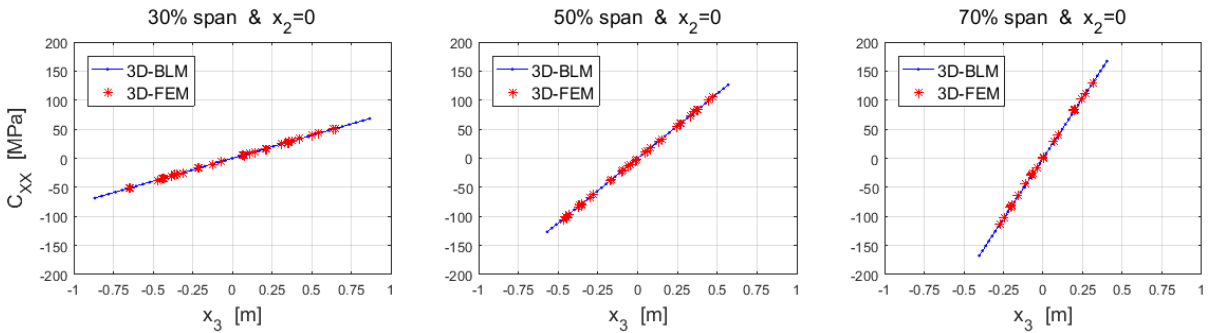


Figure 12: Longitudinal stress C_{XX} in the cross-sections at 30%, 50%, 70% span for $F=1000\text{kN}$.

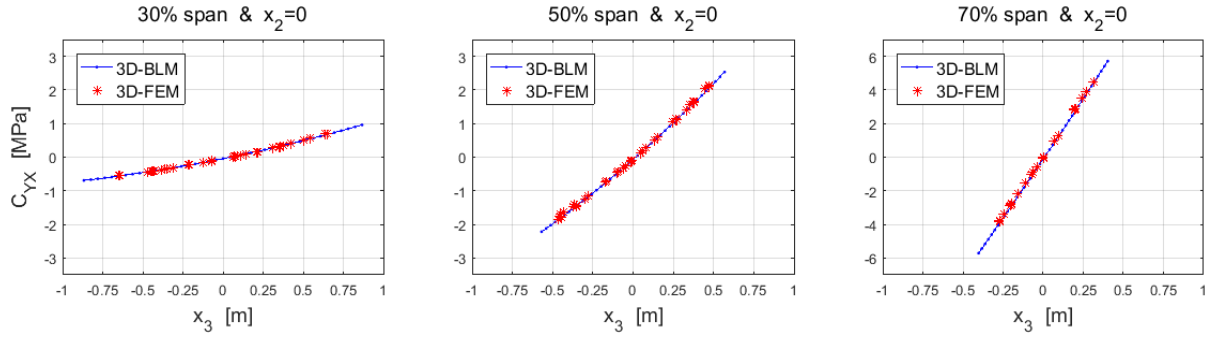


Figure 13: Transverse shear stress C_{YX} in the cross-sections at 30%, 50%, 70% span for $F=1000\text{kN}$.

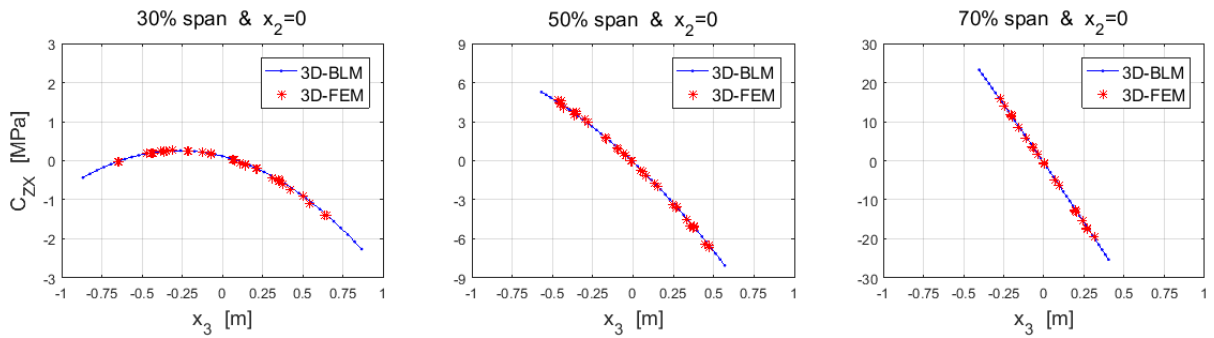


Figure 14: Transverse shear stress C_{ZX} in the cross-sections at 30%, 50%, 70% span for $F=1000\text{kN}$.

Similar results have been obtained for other tip-forces and cross-sections, confirming the effectiveness of the proposed approach but are not reported here for the sake of brevity. It is apparent, however, that the proposed model is able to generalize the results of the linear theory of prismatic beams and provides accurate results compared to 3D-FEM simulations. The approach proposed is then promising, from the point of view of design, to predict the mechanical behaviour of non-prismatic beamlike elements of interest in applications.

5 CONCLUSIONS

The design of non-prismatic beams require stress analyses that cannot be performed with the theory of prismatic beams, which would provide incorrect results because the spanwise variation in the dimensions and orientation of the cross-sections (taper and pre-twist) produces couplings between bending, twisting and tension, plus non-trivial stress distributions.

Basing on previous works, this paper investigates the effect of pre-twist on the response of bi-tapered beams, mimicking elements used in the applications. The prediction of their mechanical behaviour is reduced to finding the 3D warping of the originally transverse cross-sections and the displacements of the axis. A variational approach and the smallness of warping and strain allows expressing the 3D stress and strain in terms of some of the 1D strain

measures, 3D warping functions and geometric parameters. The approach yields analytical results that generalize those of the linear theory of prismatic beams and reduce to the latter for prismatic elements with small centre-line deflection. An efficient and accurate numerical code was implemented and tested through several comparisons with nonlinear 3D-FEM analyses.

Here we focused on the out-of-plane distortion of the cross-sections and studied the corresponding PDEs problems. Further studies will regard the in-plane cross-sections distortion and the corresponding PDEs, plus analytical investigations of the effects of the beam's curvature (superposed to those of the pre-twist and taper) on the 3D strain and stress fields.

APPENDIX

Eq. (19) provide the components F_i, M_i of the stress resultants with respect to the current local triad a_i , obtained by combining Eq. (15)-(18), which provide the strain fields (15), with Eq. (8)-(9), which relate the stress resultants (9) and the strain fields (15):

$$\begin{aligned}
 F_1 &= Y \int_{\Sigma} k_2 x_3 - k_3 x_2 + \gamma_1 + Y \int_{\Sigma} e_{1,1} + Y \int_{\Sigma} k_{B1} (x_3 e_{1,2} - x_2 e_{1,3}) \\
 F_2 &= G \int_{\Sigma} e_{1,2} - k_1 x_3 + G \int_{\Sigma} 2(1+\nu)(k_2 x_3 - k_3 x_2 + \gamma_1)(\Lambda_2^{-1} \Lambda_2' x_2 - k_{B1} x_3) + G \int_{\Sigma} e_2 \\
 F_3 &= G \int_{\Sigma} e_{1,3} + k_1 x_2 + G \int_{\Sigma} 2(1+\nu)(k_2 x_3 - k_3 x_2 + \gamma_1)(\Lambda_3^{-1} \Lambda_3' x_3 + k_{B1} x_2) + G \int_{\Sigma} e_3 \\
 M_1 &= G \int_{\Sigma} x_2 (e_{1,3} + k_1 x_2) - x_3 (e_{1,2} - k_1 x_3) + G \int_{\Sigma} x_2 e_3 - x_3 e_2 + \dots \\
 &\quad + G \int_{\Sigma} 2(1+\nu)(k_2 x_3 - k_3 x_2 + \gamma_1)[x_2 (\Lambda_3^{-1} \Lambda_3' x_3 + k_{B1} x_2) - x_3 (\Lambda_2^{-1} \Lambda_2' x_2 - k_{B1} x_3)] \\
 M_2 &= Y \int_{\Sigma} k_2 x_3^2 - k_3 x_3 x_2 + \gamma_1 x_3 + Y \int_{\Sigma} x_3 e_{1,1} + Y \int_{\Sigma} k_{B1} x_3 (x_3 e_{1,2} - x_2 e_{1,3}) \\
 M_3 &= Y \int_{\Sigma} k_3 x_2^2 - k_2 x_2 x_3 - \gamma_1 x_2 - Y \int_{\Sigma} x_2 e_{1,1} - Y \int_{\Sigma} k_{B1} x_2 (x_3 e_{1,2} - x_2 e_{1,3})
 \end{aligned} \tag{23}$$

Performing the integrals with respect to the cross-section centroid, and considering that e_1, e_2, e_3 satisfy Eq. (16)-(18), we get Eq. (19), where the coefficients multiplying 1D strains and their s -derivatives are defined as

$$A = \int_{\Sigma} 1 \tag{24}$$

$$J_0 = \int_{\Sigma} x_2^2 + x_3^2 \tag{25}$$

$$J_1 = \int_{\Sigma} (e_{1,3}^{k_1} + x_2)^2 + (e_{1,2}^{k_1} - x_3)^2 \tag{26}$$

$$J_2 = \int_{\Sigma} x_3^2 \tag{27}$$

$$J_3 = \int_{\Sigma} x_2^2 \quad (28)$$

$$J_{23} = \int_{\Sigma} x_2 x_3 \quad (29)$$

$$I_2 = J'_2 + k_{B1} J_{23} \quad (30)$$

$$I_3 = J'_3 - k_{B1} J_{23} \quad (31)$$

$$I_{23} = J'_{23} - k_{B1} J_2 \quad (32)$$

$$I_{32} = J'_{23} + k_{B1} J_3 \quad (33)$$

$$X_1 = \int_{\Sigma} e_1^{k_1} \quad (34)$$

$$Z_1 = \int_{\Sigma} e_{1,1}^{k_1} + k_{B1} (J_0 - J_1) \quad (35)$$

$$X_2 = \int_{\Sigma} x_3 e_1^{k_1} \quad (36)$$

$$Z_2 = \int_{\Sigma} x_3 e_{1,1}^{k_1} + k_{B1} \int_{\Sigma} x_3 (x_3 e_{1,2}^{k_1} - x_2 e_{1,3}^{k_1}) \quad (37)$$

$$X_3 = \int_{\Sigma} x_2 e_1^{k_1} \quad (38)$$

$$Z_3 = \int_{\Sigma} x_2 e_{1,1}^{k_1} + k_{B1} \int_{\Sigma} x_2 (x_3 e_{1,2}^{k_1} - x_2 e_{1,3}^{k_1}) \quad (39)$$

$$V_1 = \rho' \rho^{-1} \int_{\Sigma} x_2 x_3 + k_{B1} (J_0 - J_1) \quad (40)$$

$$V_2 = \rho' \rho^{-1} \int_{\Sigma} x_2 x_3^2 + k_{B1} \int_{\Sigma} x_3 (x_2^2 + x_3^2) + \int_{\Sigma} x_2 e_3^{k_2} - x_3 e_2^{k_2} \quad (41)$$

$$V_3 = \rho' \rho^{-1} \int_{\Sigma} x_3 x_2^2 + k_{B1} \int_{\Sigma} x_2 (x_2^2 + x_3^2) + \int_{\Sigma} x_3 e_2^{k_3} - x_2 e_3^{k_3} \quad (42)$$

$$H_2 = \int_{\Sigma} x_2 e_3^{k'_2} - x_3 e_2^{k'_2} \quad (43)$$

$$H_3 = \int_{\Sigma} x_3 e_2^{k'_3} - x_2 e_3^{k'_3} \quad (44)$$

where $e_j^{k_i}$ and $e_j^{k'_i}$ are the values of e_j obtained by solving Eq. (16)-(18) in the cases in which the quantity in superscript (e.g. k_2) is unitary and the others (e.g. $k_3, k'_2, k'_3, \gamma_1$) are zero.

Compliance with Ethical Standards

Funding: The financial support of University "La Sapienza" of Roma (grant no. RM11916B7ECCFCBF) and PRIN MIUR "Integrated mechanobiology approaches for a precise medicine in cancer treatment" is gratefully acknowledged.

Conflict of Interest: The authors declare that they have no conflict of interest.

REFERENCES

- [1] Goodier G.N. and Griffin D.S., Elastic bending of pretwisted bars, *Int. J. Solids Structures*, **5**, 1231-1245, 1969.
- [2] Rosen A., The effect of initial twist on the torsional rigidity of beams – Another point of view, *J. Applied Mechanics* **47**:389-392, 1980.
- [3] Hodges D.H., Torsion of pretwisted beams due to axial loading, *J. Applied Mechanics* **47**:393-397, 1980.
- [4] Krenk S., The torsion-extension coupling in pretwisted elastic beams, *Int. J. Solids Structures* **19**:67-72, 1983.
- [5] Krenk S., A linear theory for pretwisted elastic beams, *J. Applied Mechanics* **50**:137-142, 1983.
- [6] Rosen A., Theoretical and experimental investigation of the nonlinear torsion and extension of initially twisted bars, *J. Applied Mechanics* **50**:321-326, 1983.
- [7] Rosen A., Structural and dynamic behavior of pretwisted rods and beams, *American Society of Mechanical Engineers* **44**:483-515, 1991.
- [8] Kunz D.L., Survey and comparison of engineering beam theories for helicopter rotor blades, *J. of Aircraft* **31**:473-479, 1994.
- [9] Buckney N., Pirrera A., et al., On the structural topology of wind turbine blades, *Thin-walled structures* **67**:144-154, 2013.
- [10] Griffith D.T., Ashwill T.D., et al., Large offshore rotor development: design and analysis of the Sandia 100-meter wind turbine blade, *Proc. of the 53rd Structures, Structural Dynamics and Materials Conference*, April 23-26, 2012.
- [11] Migliaccio G., Ruta G., et al., Beamlike models for the analyses of curved, twisted and tapered horizontal-axis wind turbine (HAWT) blades undergoing large displacements, *Wind Energy Science*, **5**, 685-698, <https://doi.org/10.5194/wes-5-685-2020>, 2020.
- [12] Migliaccio G., and Ruta G., Rotor blades as curved, twisted, and tapered beam-like structures subjected to large deflections, *Engineering Structures*, **222**:111089, 2020.
- [13] Love A.E.H., *A treatise on the mathematical theory of elasticity*, 4th ed., Dover Publications, NY, 1944.
- [14] Simo J.C., A finite strain beam formulation, the three-dimensional dynamic problem, part I, *Computer methods in applied mechanics and engineering*, **49**, 55-70, 1985.
- [15] Ibrahimbegovic A., On finite element implementation of geometrically nonlinear Reissner's beam theory: three-dimensional curved beam elements, *Computer methods in applied mechanics and engineering* **122**:11-26, 1995.

- [16] Hodges D.H., *Geometrically exact equations for beams*, *Encyclopaedia of Continuum Mechanics*, Springer-Verlag, Berlin, 2018.
- [17] Berdichevsky V.L., On the energy of an elastic rod, *J. Appl. Mathematics and Mechanics* **45**:518-529, 1981.
- [18] Yu W., Hodges D.H., and Ho J.C., Variational asymptotic beam-sectional analysis - an updated version, *Int. J. Engineering Science* **59**:40-64, 2012.
- [19] Rosen A., and Friedmann P.P., Non-linear equations of equilibrium for elastic helicopter or wind turbine blades undergoing moderate deformation, NASA, *CR-159478*, 1978.
- [20] Ruta G., Pignataro M., Rizzi N., A direct one-dimensional beam model for the flexural-torsional buckling of thin-walled beams, *J. Mechanics of Materials and Structures* **1**:1479-1496, 2006.
- [21] Hodges D.H., Rajagopal A., et al., Stress and strain recovery for the in-plane deformation of an isotropic tapered strip-beam, *J. Mechanics of Material and Structures* **5**:963-975, 2010.
- [22] Pai P.F., Three kinematic representations for modelling of high flexible beams and their applications, *Int. J. Solids and Structures* **48**:2764-2777, 2011.
- [23] Balduzzi G., Hochreiner G., and Fussl J., Stress recovery from one dimensional models for tapered bi-symmetric thin-walled I beams: deficiencies in modern engineering tools, *Thin-Walled structures* **119**: 934-945, 2017.
- [24] Mercuri V., Balduzzi G., et al., Structural analysis of non-prismatic beams: Critical issues, accurate stress recovery, and analytical definition of the finite element (FE) stiffness matrix. *Engineering Structures*, **213**, 110252, 2020.
- [25] Migliaccio G., Ruta G., et al., Curved and twisted beam models for aeroelastic analysis of wind turbine blades in large displacements, *XXIV AIMETA conference 2019, Lecture notes in mechanical engineering*, Springer, 2020.
- [26] Hodges D.H., Review of composite rotor blades modeling, *AIAA Journal* **28**:561-565, 1990.
- [27] Rafiee M., Nitzsche F., and Labrosse M., Dynamics, vibration and control of rotating composite beams and blades: a critical review, *Thin-walled Structures* **119**:795-819, 2017.
- [28] Rubin M.B., *Cosserat theories: shells, rods and points*, Solid mechanics and its applications, Springer Netherlands, 1st ed., 2000.
- [29] Gurtin M.E., *An introduction to continuum mechanics*, *Mathematics in Science and Engineering*, Academic Press, 1st ed., 1981.
- [30] Dell'Isola F., and Bichara A., *Elementi di algebra tensoriale con applicazioni alla meccanica dei solidi*, 1st ed., Società Editrice Esculapio, Bologna, 2005.
- [31] Courant R., and Hilbert D., *Methods of mathematical physics*, Interscience Publisher, 1st ed., 1953.
- [32] Sokolnikoff I.S., *Mathematical theory of elasticity*, McGraw-Hill Inc., 1nd ed., 1946.
- [33] Timoshenko S.P., and Goodier J.N., *Theory of elasticity*, McGraw-Hill, 2nd ed., 1951.
- [34] Madenci E., and Guven I., *The finite element method and applications in engineering using Ansys*, 2nd ed., Springer, 2015.